EMBRY-RIDDLE Aeronautical University SCHOLARLY COMMONS

International Journal of Aviation, Aeronautics, and Aerospace

Volume 8 | Issue 2 Article 2

2021

Identification of Wind-Induced Hazard Zones Impacting UAS Bridge Inspection

Jack J. Green
Purdue University, green248@purdue.edu
John Mott
jhmott@purdue.edu

Within the past two decades, research on Unmanned Aerial Systems (UAS) has expanded significantly in both breadth and depth. The use of UAS for inspection of civil structures, specifically of automotive, rail, and pedestrian bridges, has recently become a topic of interest among civil engineers and other transportation stakeholders. A substantial amount of research has been conducted on general aerodynamic effects on UAS in flight. However, significant progress has yet to be made on understanding local aerodynamic impacts of civil structures on UAS flight (Sanchez-Cuevas et al., 2017). With an increase in UAS flight within urban areas, this is expected to become a topic of increasing interest.

The reduction of the degree of required human interaction in the bridge inspection process allows for increased safety not only for the inspector, but for motorists, as well. An estimated 24% increase in traffic accidents occur when an interstate lane is closed (Margreiter et al., 2017). To reduce the risk to motorists, bridge inspectors, and road crews, UAS may be utilized as an inspection platform, as they possess state of the art remote visualization capabilities as well as substantial maneuverability. This research investigates hazards created by local winds interacting with an inspected bridge structure. An aerodynamic wake is created by the bridge, in which fluid effects including wind shear, circulation, and turbulence are produced. The UAS is challenged with flying near the bridge to collect adequate data for a thorough inspection; however, these aerodynamic effects can preclude safe UAS operation.

McGrath et al. mention the existence of closed-arch recirculation vortices that exist on the aft side of a cuboid-structured building, as well as the existence of several vortex regions surrounding the same structure (2012). These commonalities exist within bridge structures as well; however, their complexities are assumed to increase the complex nature of flow areas surrounding a given bridge structure. Wang et al. have explored the different categories of wind effects on operating UAS—namely, constant wind, turbulent flow, and wind shear (Wang et al., 2019). The idea of existing flow regions allows for a description of areas surrounding a bridge structure that will be common for a given characteristic wind. Any alteration in wind direction and speed can be interpolated to examine the flow characteristics of the bridge structure within relative boundaries of wind velocity that would be experienced during a UAS flight.

External Effects on UAS

GPS-Denied Flight

As UAS are utilized in more commercial applications, e.g., civil inspection, surveying, etc., many scenarios now require performance under GPS-denied conditions. In conjunction with results shown in this research, GPS-denial can increase the magnitude of wind effects on UAS maneuverability. Research has been conducted on the effects of various building materials on GPS signal, wireless, and radio signal (Choroszucho et al., 2008). Materials commonly used in bridge

structures, including concrete, steel, and steel-reinforced concrete, show considerable effects on signal transmission, meaning that bridge structures are prone to subjecting UAS to more hazardous flight conditions (Klukas et al., 2004). Notable features impaired by these materials include mapping of surroundings, location sequencing, return-to-home functioning, fixed-space position holding, and the relay of information to the inertial sensors for overall flight control. State variables such as position, velocity, acceleration, attitude angles, and attitude rates are determined when the GPS coordinates and surrounding characteristics are relayed to the inertial sensors, and keep an operating UAS in a fixed position (Conte & Doherty, 2011). Inertial Measurement Units (IMUs) each contain a certain level of error within their measuring capabilities, and without GPS the IMU is no longer able to correct its measurement bias and will begin to drift. This drift is unbounded and increases quadratically with time if uncorrected (Chowdhary et al., 2009). UAS platforms, when in GPS-denied conditions, will attempt to stay in a fixed-position hover. However, without geolocation, and the platform will tend to drift in a manner proportional to the wind velocity. Increased turbulence will induce more erratic behavior that might not normally be observed with GPS signal availability.

UAS Platform Types

Even with the limits placed on UAS in a GPS-denied environment, flight is still possible. With a live video feed, a pilot can manually fly a UAS through enclosed spaces. The risk of platform loss under these conditions is increased; however, with appropriate training, and weighing of risks by stakeholders, an inspection may be completed successfully. Further technologies are being developed to make successful GPS-denied flight obtainable. The types of UAS platforms chosen for bridge inspection will play a vital role in determining the overall safety of an operation. Ideally, these platforms will be maneuverable enough to traverse tighter spaces some bridge types may impose. A plate girder bridge, for example, sometimes only gives a few feet of space between girders, which are a pivotal point during current bridge inspection. Additionally, these platforms would have imaging capabilities on par with high end cameras, as to capture small details that otherwise might be missed by low quality cameras. Several common platforms used for imaging and data acquisition exist, however the use of any particular platform is beyond the goals and scope of this research.

Heat-Convection Above Roadways

Wind shear effects create a large potential for hazardous UAS operations; however, further analysis on convection effects of road surfaces is needed in order to understand the nature of airflow above a bridge structure. This convection may inhibit the ability for a structured vortex pocket to form, while it also may induce greater turbulent effects on the top side of a bridge deck.

Environmental Effects on Vehicle Forces and Moments

Increased wind velocity causes an increase in required power from UAS motors to maintain stable and level flight. Because of this, it is expected that on days with wind exceeding 2 m/s, maximum flight times will be shortened significantly, as the greater thrust required from the rotors due to the instability of the system decreases the endurance of the craft. For a one Newton increase in thrust, the flight time can decrease by more than 50% (Ranquist et al., 2017). It is important to note that the decrease in flight time will manifest as the UAS encounters turbulence around a bridge structure.

Proximity to Structures

Sanchez-Cuevas et al. provide an explanation of whether the classical model of ground effect developed for larger-rotor aircraft is upheld in smaller-rotor aircraft (2017). Their research suggests that in scenarios where ground effect is the only aerodynamic interruption, the classical model is relevant and accurate in predicting the thrust behavior of UAS. Experimentation shows that ground and ceiling effects on a UAS are substantial within a few meters from those surfaces. These effectively create additional thrust for the UAS, causing it to be pushed or pulled from a surface beneath or above it, respectively. The ground effect combined with additional wall effects can prove to be more chaotic than ground effect alone, resulting in a greater risk of blade flapping and unstable flight (Huang et al., 2009). Ceiling effects pull a UAS toward a surface above the craft, requiring additional caution when flying underneath a surface, so as to reduce the risk of a collision with the ceiling. The existence of external wind creates shearing and circulation near the wall, as well. Erratic wind behavior has a high potential for inhibiting controlled flight in severe wind conditions. It is worth noting that current UAS platforms are capable of obstacle avoidance with available sensors and inertial measurement units (IMU). The issue of standoff capability, defined here as the ability of a UAS to operate at a certain distance from the inspected specimen, is well addressed outside of this research (Duran et al., 2020). Here, it is assumed that a UAS is required to operate within potential hazard zones due to current image capturing capabilities of existing UAS platforms (Seo et al., 2018).

Mitigation of Hazard Zones

To successfully traverse a bridge structure and obtain the imaging required for adequate inspection, alternative plans may be developed by the pilot to ensure that the UAS may be operated safely. It is possible that imaging of bridge components that lie within a hazard zone might require the UAS to operate adjacent to the hazard zone. It is also feasible that a pilot would place the UAS on an alternate path such that the hazard area is avoided entirely. It is worth noting that inspection protocols are expected be instituted based on the needs of state Departments of Transportation, as well as the needs of the UAS operator established by the FAA. FAA 14 CFR Part 107 stipulations do not specify regulations for UAS-based inspection flights; however, all existing general regulations must be followed.

Currently, FAA support for commercial inspection flight can be obtained via a certificate of authorization (COA), or other alternative action waiver (FAA).

Research Methodology

Computational Fluid Dynamics (CFD) offers the ability to mathematically and visually understand the impacts of surface boundaries on flow particles passing through a given region, given an initial wind velocity based in cartesian coordinates. Various velocities are analyzed to develop an understanding of the severity of potential hazards, and whether they exist within a specific range of wind velocities. For this research, analysis of wind velocities of 2 m/s, 5 m/s, 10 m/s, and 15 m/s are conducted. As the vast majority of UAS models are suggested to operate under 30 miles per hour (13.4 m/s), a limit of 15 m/s (33 mph) is used as the maximum simulation velocity. Further regulation on UAS-based bridge inspection will determine the allowance of flight in various wind conditions.

CAD Model

The bridge structure analyzed in this research is modeled after the US 52 westbound bridge in Lafayette, Indiana. The plate-girder bridge runs alongside another bridge carrying eastbound traffic. For simplicity, an analysis of only one of these overpass structures is conducted. Pictures and publicly available data facilitated the creation of a proportionately representative Computer Assisted Design (CAD) model using Solidworks 3D CAD software. While perfectly exact bridge measurements are not utilized for the model, it is believed to provide a sufficiently accurate representation for the purposes of this study.

CFD Simulation Parameters

The software used to conduct this analysis is SimScale computer-aided engineering software, chosen for the application of either a steady-state or transient analysis to flow simulations, as well as the ability to test various turbulence models. For this simulation, a k-omega SST turbulence model is applied in conjunction with steady-state time dependency. Although results of previous CFD simulations show that both the k-omega and k-epsilon turbulence models are capable of accurate, generalizable, and appropriate results, it is suggested that the k-omega SST turbulence model be used for lower Reynolds number scenarios, such as a moderate wind velocity acting across a large structure surface (Anderson, 2010).

The placement of “probe points” anywhere in the Cartesian coordinate system provides calculated values for the parameters that are to be analyzed; specifically, vectored wind velocity, turbulent kinetic energy (TKE), and specific dissipation rate (SDR). TKE and SDR, when analyzed over the simulation time, show the energy and behavior associated with eddies within this region. This provides a computational model for turbulence. The TKE of a given point will obtain a higher value when the fluid field in that region holds greater kinetic energy, and in conjunction with a high value for kinetic dissipation, yields a higher turbulence property for the selected point. TKE is calculated by determining the

measured root-mean-square (RMS) velocity fluctuations. The RMS of these fluctuations show exactly how the energy is dispersed over a given velocity field. SDR is directly related to TKE, as it is the rate at which TKE is converted into thermal internal energy. Common understanding of CFD models suggests that there is no strict mathematical definition for SDR, however the general conversion-rate theory is used amongst common CFD models (Kumer et al., 2016). The locations of the probes relative to the bridge deck are shown (Figure 1).

Figure 1

Visualization of Probe Points Selected around Overpass Bridge Structure, within 10 m/s Flow Field

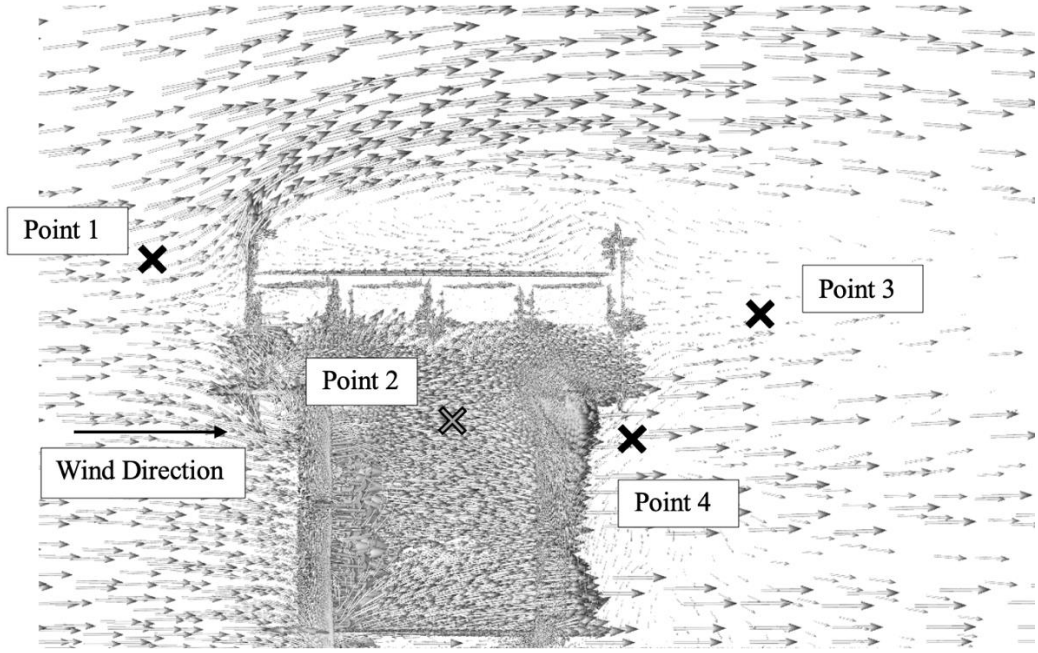

›

The “probes” are placed within the simulation in various spots surrounding the bridge deck. The probe points are selected to represent potential hazard zones that yield the least predictable results based on previous research. Additionally, probe points are placed extending behind the bridge deck (relative to wind origin) to visualize how far an adverse flow pocket extends behind the deck. This pocket is theorized to extend until the separated streamlines reattach. Initial assessment of streamlines within the simulated flow field indicated regions of interest near the bridge structure. A previous simulation displaying a colorized velocity field reveals consistent areas of wind shear, vortex columns, streamline separation and reattachment, as well as recirculation cylinders downstream of the bridge deck.

Simulation Results

Results are compiled in three sections of analysis: the wake induced by the bridge, turbulence surrounding the bridge structure at various wind speeds, and the wind shear above and below the bridge deck. These sections explain the most profound areas of wind-induced hazards from the results of this research. While each has implications on UAS flight safety, they are not an exhaustive list of hazards a UAS may face in bridge inspection flight.

Bridge Wake

When analyzing the velocity changes for a probe point placed two meters behind the bridge deck, one can see the fluctuation in velocity that occurs as a result of the turbulent flow (Figure 2). The large variability of the velocity at this point indicates greater turbulence. It is worth noting that the initial wind velocity in this case is 5 m/s, and the data is collected over a 120-second simulation. The average velocity of just over 0.5 m/s indicates that adverse flow is common within this region. Additionally, spikes in wind velocity suggest that greater values of TKE and SDR are anticipated.

Figure 2

Z-Velocity Component Measured at Probe Point 5, m/s

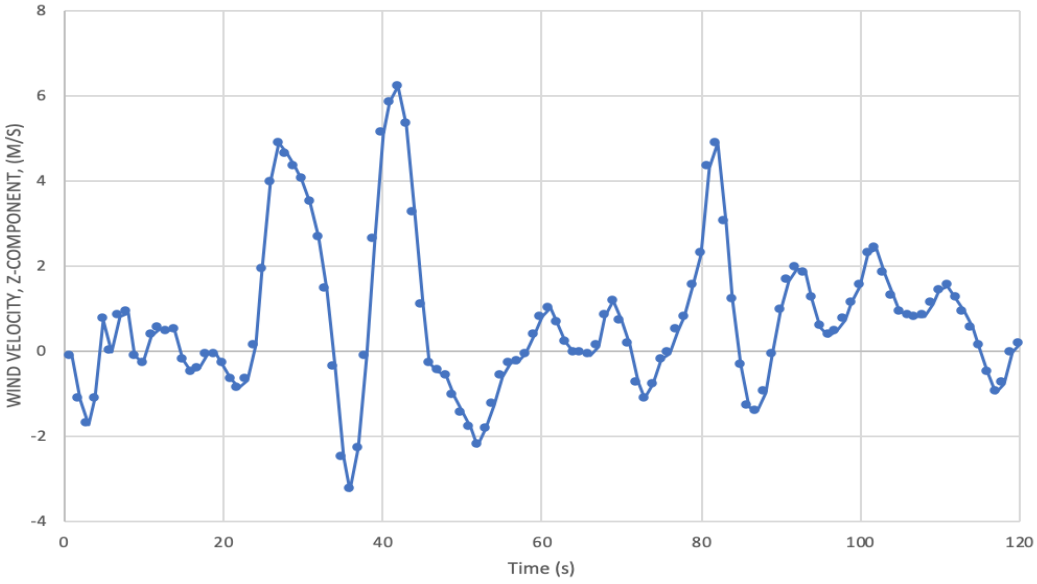

Figure 3

Velocity Vector Field Visualization and Probe Point Positioning, 5 m/s

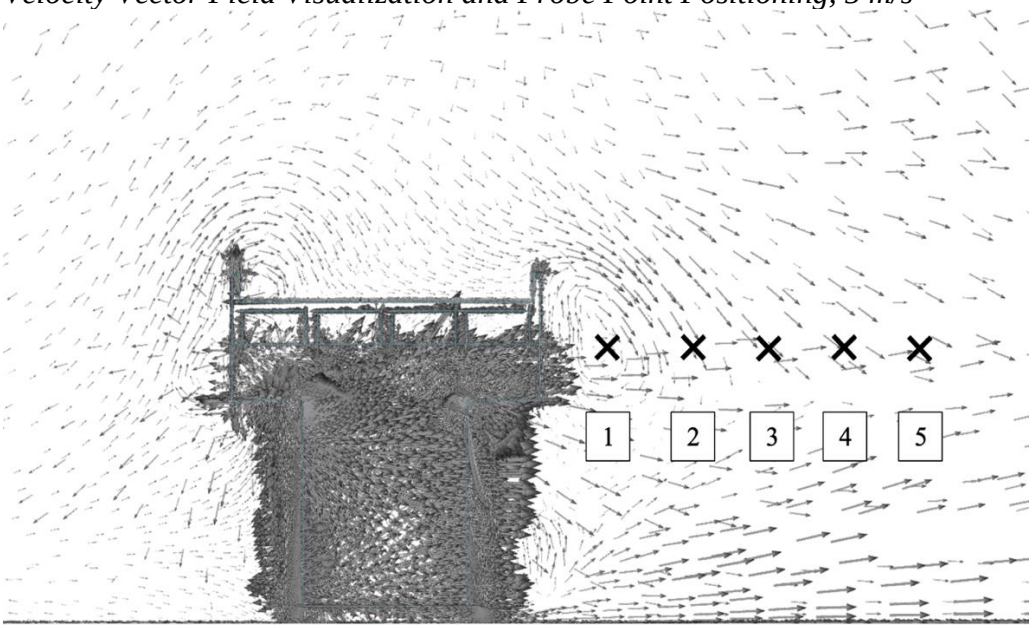

Four other probe points placed in positions extending behind the bridge deck relative to the wind velocity origin show the differences in both velocity fluctuations and turbulence characteristics (Figure 3). Increasing the simulation wind speed increases the difference between point velocities, with probe points further from the bridge deck experiencing a greater wind velocity. The probe points closer to the bridge deck remain within an adverse flow region (Table 1). This pocket of adverse flow, extending to at least 2 meters beyond the bridge deck, is created by a pressure differential that pulls the flow in. At higher wind velocities, this pocket is lengthened due to the wind shear extending from on top of to below the bridge deck, and is further analyzed below. In visualizations of flow animation, this pocket can be seen to oscillate at each initial wind speed, indicating the presence of turbulence. The turbulence also appears to grow as wind speed increases.

Table 1

Point Characteristics behind Bridge Deck, 5 m/s

Stability Analysis of Points, 5 m/s					
Probe Point #	1	2	3	4	5
Average Velocity (m/s)	-0.6731	-0.6731	0.9710	4.2414	4.0216
Standard Deviation	1.7904	1.7904	2.8164	5.3673	4.8304
Average TKE (m^2/s^2)	0.6952	0.6952	0.9750	4.2854	4.0633
Max TKE (m^2/s^2)	6.2001	6.2001	6.0053	6.3033	6.4004
Average SDR (1/s)	11.4946	11.4946	9.4522	8.1296	6.5223
Max SDR (1/s)	19.8893	19.8893	15.2140	12.5402	10.2165

The data confirms the existence of turbulence and circulation near the bridge deck. While the average TKE values are lower than those seen farther away, nearing 0.6 m^2s^{-2}, the higher SDR values found at points 1 and 2 suggest well-formed circulation. Here, the kinetic energy of the model is being dissipated into circulation; however, a greater specific dissipation rate is consistent with continued air movement in a turbulent nature.

Higher average TKE, with maximum reaching as high as 6.4 m^2s^{-2} in some cases, in conjunction with still-elevated SDR values suggests an increase of turbulence at points farther downstream. This is thought to result from the reattachment of streamlines separated previously by the bridge structure. Because this air appears to be unstable, a potential for hazard arises; however, the increased distance from the bridge deck or other surrounding structure gives a UAS additional maneuvering room in the event adverse conditions are encountered.

Bridge-Induced Turbulence

A series of points surrounding the bridge structure, shown previously in Figure 1, allows for various characteristic wind effects to be analyzed. These points, as mentioned earlier, are selected such that they are both within close proximity to the structure to represent potential areas of UAS flight, and function as areas where flow is anticipated to behave more unpredictably. Fluctuation in velocity indicates turbulent behavior, so values of velocity for each of these points are included (Table 2).

Table 2
Probe Point Velocities

Probe Point Characteristics				
Probe Point #	1	2	3	4
Average Velocity (m/s)	5.7926	12.3153	0.7370	-1.0310
Standard Deviation	0.5650	0.5891	0.2583	0.5454
Average TKE (m^2/s^2)	0.1584	0.0495	0.7010	2.2737
Max TKE (m^2/s^2)	0.8285	0.5330	1.7200	2.6769
Average SDR (1/s)	3.8805	1.7441	9.9020	7.1577
Max SDR (1/s)	10.0888	7.3169	14.1843	20.1504

It is interesting to note that Point 4, located at the corner where the bridge deck and pier meet, shows the greatest velocity fluctuation. This indicates that turbulence is prominent in this region. The data shows this section contains both the highest TKE and SDR values of 2.67 m^2s^{-2}, and 20.15 s^{-1}, respectively. It is also worth noting that with an average velocity of -1.03 m/s, this point experiences regular adverse flow as a result of the lower pressure behind the bridge piers. A higher SDR (9.9 s^{-1}) is also present at Point 3, located directly behind the bridge deck, beneath the shear line. This point has the lowest average velocity at 0.74 m/s; however, the larger SDR value suggests that turbulence is also prominent at this point. The lower velocity average indicates the adverse flow that is expected within the shear pocket described previously. Points 1 and 2 exhibit the lowest variation in velocity, which is expected from their locations. Point 1 experiences steady flow that has yet to be interrupted by the bridge deck, while Point 2 exists within the separated streamlines under the bridge deck. Point 2 shows the highest velocity average of over 12 m/s. This is worth noting, as the simulation was conducted using an initial wind speed of 10 m/s, indicating a Bernoulli effect on the bridge structure.

Wind Shear

The placement of probe points above and below the anticipated shear boundary that exists in moderate to severe wind conditions allows for hazard analysis within this region. The points are placed at the following positions, indicated by boxed numbers (Figure 4):

1. In front of bridge deck, prior to wind interaction (free stream flow analysis)
2. 0.5 meters above shear line, within free stream flow existing above the bridge deck
3. 0.5 meters below shear line, within adverse flow region created by pressure differential

Figure 4

Wind Shear Probe Point Indication

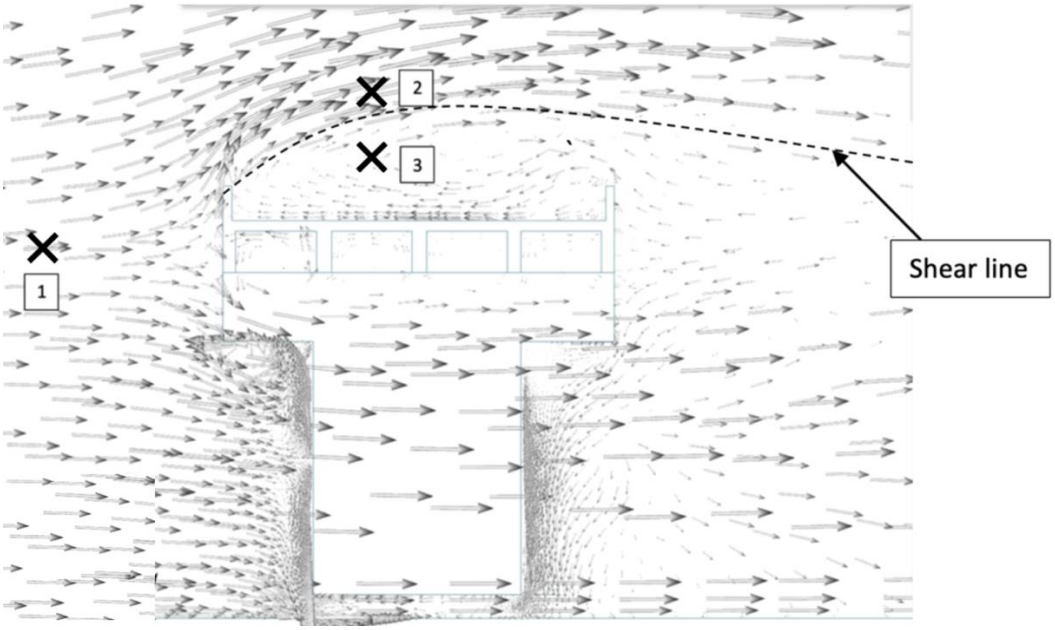

Above a bridge deck, UAS will experience higher wind velocities than the free stream velocities. Just 1 m toward the bridge deck, adverse flow is experienced, creating a moment upon the aircraft, indicating the need for stabilization. At extreme wind speeds close to UAS manufacturer wind limits, this moment could be sufficient to result in control loss, and may require extensive pilot control input if the UAS is unable to stabilize itself. It is seen that at wind speeds nearing 10 m/s the wind gradient over only a meter can become extreme, with a 12.6 m/s difference in wind speed between two points only 1 meter apart. (Table 3).

Table 3

Velocity Differential between Shear Zone and Adverse Flow

Wind Shear Region Velocities					
1	Free Stream Speed (m/s)	2 m/s	5 m/s	10 m/s	15 m/s
2	Shear Zone Speed (m/s)	1.75	3.75	11.73	16.35
3	Adverse Flow Speed (m/s)	1.03	2.72	-0.87	-1.79
	Difference (m/s)	0.72	1.03	12.6	18.14

The compression of streamlines flowing above the bridge deck reduces the area through which the air mass can travel, increasing the flow velocity, consistent with Bernoulli's Principle. Although this increase in speed is not evident until wind

velocities are in excess of 10 m/s, the more-than 10% increase in wind speed is felt one meter closer to the bridge. Adverse flow, reaching as far as -2 m/s in some areas in both the 10 m/s and 15 m/s simulations, creates a large gradient in just a matter of 1 to 2 meters. An 18.14 m/s difference in velocity is experienced within 1 meter of flight at a 15 m/s wind velocity.

Extended Wind Shear Effects

Wind shear is a potential hazard that also results from airflow interactions with the bridge structure. The free stream flow continues to extend past the bridge deck while lower pressures directly behind the bridge deck create another adverse flow zone. This zone extends beyond the bridge deck, with its length depending on the free stream wind velocity, as well as the shape of the overpass bridge deck. Analysis of probe points can determine the characteristics of the flow field extending beyond the bridge deck. Probe points are aligned as shown previously in Figure 3.

Table 4

Velocities within Aftward Wind-Shear Pocket

	Average Wind Velocity (Z-direction) (m/s)			
Point distance from bridge deck (m)	2 m/s	5 m/s	10 m/s	15 m/s
0.5	-0.13	0.24	-0.33	-1.16
2	-0.11	0.31	-0.38	-1.14
4	-0.09	0.23	-0.92	-1.42
6	0.63	2.56	3.21	5.85
8	0.72	3.78	3.88	7.06
12	1.12	4.23	7.85	13.84

Results indicate that the pocket of adverse flow exists behind the bridge deck and is dependent on the initial wind velocity (Table 4). An adverse flow of -1 m/s is common for at least 4 meters at 15 m/s freestream wind velocity. This pocket is a similar length at 10 m/s freestream wind velocity; however, the area of streamline reattachment beyond the adverse flow pocket indicates slower velocities than that of higher wind speeds. At lower initial wind speeds, a pocket is not well formed, although turbulent flow is present.

Discussion of Results

The research shows that higher values of TKE and SDR are found where well-formed circulation exists behind the bridge piers, behind the bridge deck, and at the connecting joints where the piers meet the bridge deck. This circulation reaches higher values of TKE (greater than 4 m^2s^{-2}) at wind speeds as low as 5 m/s. Kumer

et al. show that TKE values of 4 m^2s^{-2} or above are consistent with wind gusts. Figures 5 and 6 show simulation results in the form of vectorized arrows showing wind speed at various points surrounding the bridge deck, with larger arrows represent a higher wind velocity (2016). It is clear that certain areas surrounding the bridge deck show several of the characteristic flows discussed previously (Figure 5).

Figure 5

Visualization of Wind Flow Velocity Vectors Surrounding Bridge Structure, 10 m/s

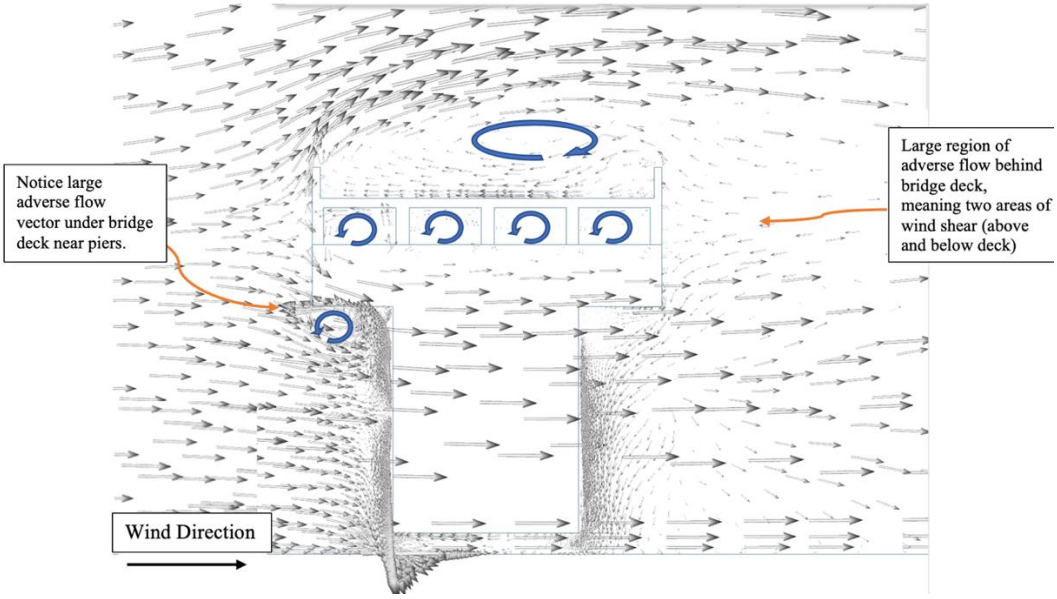

A closer look at the velocity vectors surrounding the bridge deck clarify the rotational areas within the deck spans, as well as the rotation occurring to the left of the pier in the image. The counterclockwise rotation under the bridge deck and to the left of the piers is substantial at the simulated 10 m/s wind velocity. This rotation is also present on the aft side of the bridge deck behind the pier. Rotation in these spots is significant, as it limits the ability of a UAS to areas access those areas for inspection.

Previous research has suggested that the successful use of UAS-mounted imaging devices depends not only on the quality of the devices, but on the platform stability, as well (Hallermann et al., 2016). As a result, alternative inspection methods may be needed when turbulence is present, such as when higher wind velocities in directions perpendicular to the bridge deck exist. With greater circulation and vorticity in these situations, the likelihood of platform instability and loss of control increase, and the UAS could be at risk of collision with the bridge structure (Pinto et al., 2021). Figure 6 presents a generalized depiction of an integrated hazard model.

Red areas depict spatial regions in which any of the following occur:

- A velocity gradient exceeds 5 m/s within 1 meter of flight path,
- TKE and SDR reach values indicating significant turbulence, or
- Proximity to the bridge structure reaches a point where localized effects promote collision

Orange areas depict regions that exhibit any of the following:

- Proximity to bridge structure could be altered without caution of UAS position,
- Velocity gradient reaches a value between 2 and 5 m/s within 1 meter of flight path, or
- TKE and SDR reach values indicating moderate turbulence

Figure 6

Identification of Hazard Zones for 10 m/s Wind Velocity

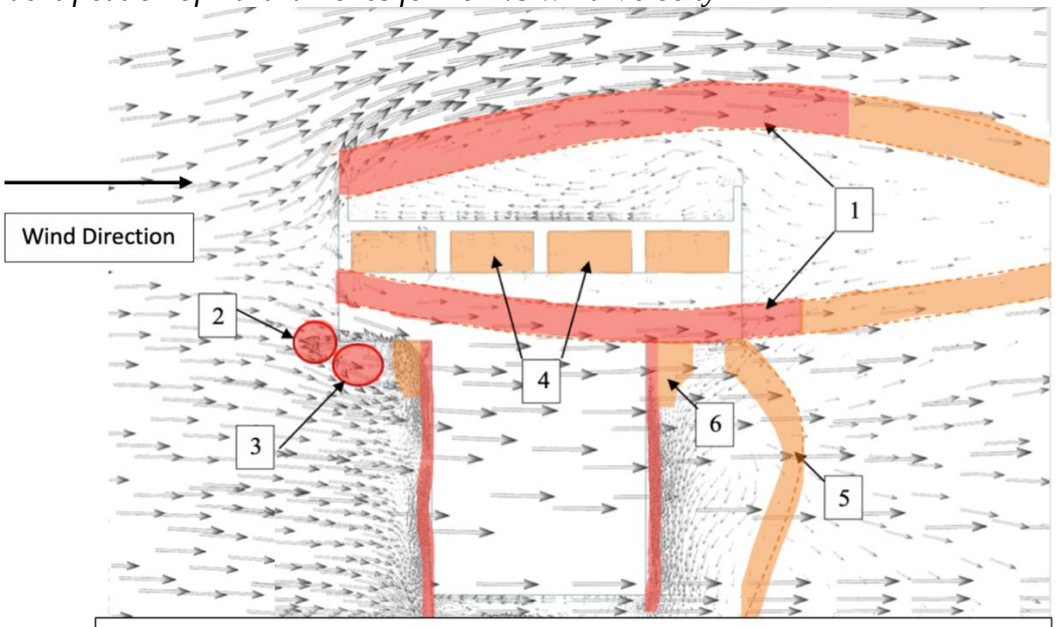

Identification of hazard zones nearby a bridge structure.

1. Wind Shear gradient regions
2. Strong adverse flow resulting from region circulation
3. Well-formed circulation resulting from pier-bridge deck connection, windward side
4. Circulation in areas between bridge span trusses
5. Vortex layer extending behind piers
6. Well-formed circulation resulting from pier-bridge deck connection, aft side

Conclusions

This paper describes several identifiable effects of wind that may potentially create hazards for operating UAS inspection platforms. Results presented herein suggest that the identified UAS-flight hazard areas exist within close proximity to

a bridge at several locations. At even moderate wind speeds between 5 and 10 m/s, wind shear becomes a potential hazard directly above and below the bridge deck, causing an effective moment on operating UAS platforms passing through this zone. This moment can degrade the stability of the aircraft, possibly inducing a loss of control. Wind shear effects also extend beyond the bridge deck, creating a pocket of adverse flow downstream of the deck. The intensity of turbulence in this region increases proportionately with wind speed.

Additional locations of circulation and turbulence exist in front of and behind bridge piers. Larger values of turbulent kinetic energy and specific dissipation rate suggest that these regions harbor greater turbulence, and ultimately greater hazards for UAS flight. Circulation resulting from the airflow develops to a substantial level at just 5 m/s of applied external wind, creating a one-meter region of circulation at the corner of the bridge deck and pier connection. The unpredictability of the circulation of air indicates that wind speeds in excess of 5 m/s would make this region a less-than-optimal zone for UAS flight (Ranquist et al., 2017). The force vectors associated with these areas can increase to a large enough magnitude that the UAS is at risk of permanent control loss at wind speeds ranging from 5 to 10 m/s (Pinto et al., 2021).

While not possible to include operating ranges for every UAS platform, further understanding of which platforms would be most affected by the wind hazards presented here will prove significant in developing protocol for UAS-based bridge inspection. Many platform types exist, ranging in size, maneuverability, imaging capabilities, and data transmission. It is possible to conclude that some platforms will be more highly impacted from the described hazards, however specific safe ranges will depend heavily on the wind conditions and parameters of the operating UAS.

Future Work

Further research may be helpful in determining the extent of the hazards described herein, and should include field testing using UAS platforms and some means of extrapolating wind vector field data. This may include, but is not limited to, the creation of a UAS flight performance model that predicts hazard potential based on UAS platform, as well as bridge and wind type. The growth of knowledge in this area will no doubt be beneficial to the development of bridge inspection protocols. Additional research may also be helpful in suggesting how traffic and road conditions, specifically convective heating, affect the airflows analyzed here. Finally, it is anticipated that field measurements will lead to simulation model refinement, potentially allowing the extension of the model described here to other areas of civil infrastructure inspection.

References

Anderson Jr, J. D. (2010). *Fundamentals of aerodynamics*. Tata McGraw-Hill Education.

Choroszucho, A., Pieńkowski, C., & Jordan, A. (2008). Electromagnetic wave propagation into building constructions. *Przegląd Elektrotechniczny, 84*(11), 44-49.

Chowdhary, G., Ottander, J., Salaun, E., & Johnson, E. (2009). Low cost guidance, navigation, and control solutions for a miniature air vehicle in GPS denied environments. In *Proceedings of 1st Symposium on Indoor Flight Issues, Mayaguez, Puerto Rico* (p. 12).

Conte, G., & Doherty, P. (2011). A visual navigation system for UAS based on geo-referenced imagery. *International Archives of the Photogrammetry, Remote Sensing and Spatial Information Sciences, 38*(1/C22). https://doi.org/10.5194/isprsarchives-XXXVIII-1-C22-101-2011

Duran, D., Johnson, M., & Stansbury, R. S. (2020, April). Towards collaborative obstacle avoidance using small UAS in indoor environments. In 2020 IEEE/ION Position, Location and Navigation Symposium (PLANS) (pp. 1596-1605). IEEE. doi:10.1109/PLANS46316.2020.9110141

Federal Aviation Administration. *Fact sheet: Small unmanned aircraft regulations (Part 107)*. Author. https://www.faa.gov/news/fact_sheets/news_story.cfm?newsId=22615. Accessed Apr. 15, 2020.

Hallermann, N., Morgenthal, G., & Rodehorst, V. (2015, September). Unmanned aerial systems (UAS)–Survey and monitoring based on high-quality airborne photos. In *IABSE Symposium Report* (Vol. 105, No. 22, pp. 1-8). International Association for Bridge and Structural Engineering.

Huang, H., Hoffmann, G. M., Waslander, S. L., & Tomlin, C. J. (2009, May). Aerodynamics and control of autonomous quadrotor helicopters in aggressive maneuvering. In *2009 IEEE international conference on robotics and automation* (pp. 3277-3282). IEEE. doi:10.1109/ROBOT.2009.5152561

Klukas, R., Julien, O., Dong, L., Cannon, E., & Lachapelle, G. (2004). Effects of building materials on UHF ranging signals. *GPS solutions, 8*(1), 1-8. doi:10.1007/s10291-003-0080-4

Kumer, V. M., Reuder, J., Dorninger, M., Zauner, R., & Grubišić, V. (2016). Turbulent kinetic energy estimates from profiling wind LiDAR measurements and their potential for wind energy applications. *Renewable Energy, 99*, 898-910. https://doi.org/10.1016/j.renene.2016.07.014

Margreiter, M., Imhof, H., Grosanic, S., & Motamedidehkordi, N. (2017). Effects of short-term lane closures on traffic flow of freeways. In *Transportation Research Board 96th Annual Meeting Compendium of Papers*.

https://www.researchgate.net/publication/312472366_Effects_of_Short-Term_Lane_Closures_on_the_Traffic_Flow_of_Freeways

McGrath, B. E., Cybyk, B. Z., & Frey, T. M. (2012). Environment-vehicle interaction modeling for unmanned aerial system operations in complex airflow environments. *Johns Hopkins APL Technical Digest*, *31*(2), 115-131. https://www.jhuapl.edu/Content/techdigest/pdf/V31-N02/31-02-McGrath.pdf

Pinto, J. O., Jensen, A. A., Jiménez, P. A., Hertneky, T., Muñoz-Esparza, D., Dumont, A., & Steiner, M. (2021). Real-time WRF large-eddy simulations to support uncrewed aircraft system (UAS) flight planning and operations during 2018 LAPSE-RATE. *Earth System Science Data*, *13*(2), 697-711. https://doi.org/10.5194/essd-13-697-2021

Ranquist, E., Steiner, M., & Argrow, B. (2017, January). Exploring the range of weather impacts on UAS operations. In *18th Conference on Aviation, Range and Aerospace Meteorology, Seattle, WA*.

Sanchez-Cuevas, P. J., Heredia, G., & Ollero, A. (2017, November). Experimental approach to the aerodynamic effects produced in multirotors flying close to obstacles. In *Iberian Robotics Conference* (pp. 742-752). Springer, Cham. https://doi.org/10.1007/978-3-319-70833-1_60

Sanchez-Cuevas, P., Heredia, G., & Ollero, A. (2017). Characterization of the aerodynamic ground effect and its influence in multirotor control. *International Journal of Aerospace Engineering*, *2017*. https://doi.org/10.1155/2017/1823056

Seo, J., Duque, L., & Wacker, J. P. (2018). Field application of UAS-based bridge inspection. *Transportation Research Record*, *2672*(12), 72-81. https://doi.org/10.1177/0361198118780825

Wang, B. H., Wang, D. B., Ali, Z. A., Ting Ting, B., & Wang, H. (2019). An overview of various kinds of wind effects on unmanned aerial vehicle. *Measurement and Control*, *52*(7-8), 731-739. https://doi.org/10.1177/0020294019847688